Available online at www.sciencedirect.com
ScienceDirect
Trans. Nonferrous Met. Soc. China 32(2022) 448−460
Transactions of Nonferrous Metals Society of China
www.tnmsc.cn

Corrosion and pitting behavior of pure aluminum 1060 exposed to Nansha Islands tropical marine atmosphere

Can PENG[1,2], Yu-wei LIU[2,3], Ming-xiao GUO[1,2], Tian-zhen GU[1,2], Chuan WANG[2,3], Zhen-yao WANG[2,3], Cheng SUN[2,3]

1. School of Materials Science and Engineering, University of Science and Technology of China, Shenyang 110016, China;
2. Institute of Metal Research, Chinese Academy of Sciences, Shenyang 110016, China;
3. Liaoning Shenyang Soil and Atmosphere Corrosion of Material National Observation and Research Station, Shenyang 110016, China

Received 19 March 2021; accepted 26 October 2021

Abstract: The corrosion and pitting behavior of pure aluminum 1060 exposed to Nansha Islands marine atmosphere for 34 months was investigated based on mass loss measurement, scanning electron microscopy (SEM), energy dispersive spectroscopy (EDS), X-ray photoelectron spectroscopy (XPS), and electrochemical impedance spectroscopy (EIS). The results indicated that serious pitting corrosion occurred on the surfaces of pure aluminum. The corrosion rate after exposure for 13 months was approximately 1.28 g/(m^2·a). The XPS results showed that the corrosion products were Al_2O_3, $Al(OH)_3$, and $AlCl_3$. Moreover, the corrosion product layer was more protective than the native oxide film, and the protectiveness first increased and then decreased. Finally, the shape of the pits was evaluated using statistical analysis.
Key words: aluminum; atmospheric corrosion; Nansha Islands; pitting corrosion; field exposure

1 Introduction

Nansha Islands are located in a crucial geographical location in the southern part of the South China Sea. Over the past several years, China has built a considerable amount of infrastructure on the islands, such as lighthouses, maritime search bases, hospitals, and airports for cases of emergencies. The working environment of these facilities in Nansha Islands, however, is characterized by high temperatures, high humidity, and high salt levels, which represents a typical harsh marine atmospheric environment [1,2]. Several field exposure corrosion tests show that metal material undergoes serious corrosion in marine atmosphere [3−6].

Aluminum and aluminum alloys are commonly used in buildings, electrical engineering, and transportation owing to their excellent performance, good mechanical properties, low weight, and corrosion resistance [4]. Pure aluminum presents good corrosion resistance owing to the formation of a protective oxide film [7,8]. It is widely accepted that, however, in marine atmosphere, high relative humidity and high chlorides deposition rate can increase the corrosion rate of aluminum. In Nansha Islands, the relative humidity is as high as 81.6%, which makes it easy to reach the deliquescence relative humidity of chlorides, leading to forming a thin water film on surfaces of the samples to accelerate corrosion [9−11].

Pitting corrosion is the main and most damage

Corresponding author: Chuan WANG, Tel: +86-18842464777, E-mail; cwang@imr.ac.cn;
Zhen-yao WANG, Tel: +86-13082423466, E-mail: zhywang@imr.ac.cn
DOI: 10.1016/S1003-6326(22)65806-0

type of corrosion for aluminum alloys in the marine atmosphere [8]. The main reason is that the oxide film formed on aluminum in its natural state has a positive surface charge and can absorb Cl^-. The absorbed Cl^- has a small radius, and can penetrate through the oxide film, then pitting corrosion occurs at the metal substrate/oxide film interface [12]. Pitting corrosion is a complex process that is affected by various factors, including the type of aggressive ions in the solution and their concentration, temperature, time of wetness, and structural characteristics of the native oxide film [4,5,11,13,14]. Numerous studies, both laboratory simulation acceleration tests and field exposure corrosion tests, have reported the pitting corrosion behavior of pure aluminum and aluminum alloys in the presence of chlorides. CUI et al [11] studied the corrosion behavior of pure aluminum 1060 in Xisha marine atmosphere and concluded that the higher chloride deposition rates and anoxic conditions created by the large-scale presence of corrosion products were critical reasons for the continuous rise in pit depth with an increase in exposure time. RODRÍGUEZ et al [15] investigated the pitting corrosion behavior of aluminum under different environmental conditions near the coastline, and found that the pitting corrosion was severer at locations with higher chloride contents. CAO et al [16] researched the electrochemical corrosion behavior of 2A02 aluminum alloy under an accelerated simulated marine atmosphere and concluded that protective corrosion products could reduce the corrosion rate.

Generally, aluminum and aluminum alloys are prone to pitting corrosion in the medium-containing Cl^- [17]. To better understand the reason and process of pitting corrosion, we need to acquire more data, such as the types of pits, and understand how the Cl^- interacts with oxide film to cause it destruction. In addition, pitting corrosion is a random event. It is necessary to examine it using some statistical methods. Although the corrosion behavior of aluminum and aluminum alloys has been a very old topic and a vast number of people have carried out detailed researches, the corrosion behavior varies significantly in different environments. Many factors affect atmospheric corrosion, and field exposure corrosion tests can provide us more real and reliable information.

Presently, aluminum and aluminum alloys are widely used in Nansha Islands, whereas no information regarding their corrosion is available. Therefore, it is necessary to conduct the relevant research. In this work, the corrosion behavior and mechanism of pure aluminum 1060 exposed to Nansha Islands marine atmosphere were investigated by mass loss, electrochemical impedance spectroscopy (EIS), scanning electron microscope (SEM) and energy dispersive spectroscopy (EDS), combined with X-ray photoelectron spectroscopy (XPS) and white-light interferometer (MicroXAM). The results of this study provide a detailed comprehension on the corrosion behavior of pure aluminum in the tropical marine atmosphere.

2 Experimental

2.1 Materials and field-exposure conditions

The experimental material was AA 1060 pure aluminum plates with sizes of 200 mm × 100 mm × 5.5 mm. The composition of the plates is shown in Table 1. Before the tests, the surfaces of the samples were degreased with acetone, rinsed with deionized water, and dried in a stream of cold air. The prepared samples were then immediately stored in a desiccator prior to use.

Table 1 Chemical composition of pure aluminum 1060 (wt.%)

Si	Fe	Cu	Mn	Mg	Zn	Ti	Al
0.13	0.15	0.03	0.01	0.01	0.02	0.01	Bal.

The exposure site was in Mischief Reef of Nansha Islands (northern latitude 9°54′, eastern longitude 115°32′), 150 m away from the coastline, belonging to the typical tropical marine atmospheric environment. All samples were exposed from September 1, 2017. The aluminum plates faced south at an angle of 45° with the horizontal plane. After 5, 13, 21 and 34 months of exposure, four parallel samples were retrieved. The main environmental parameters of the exposure site are listed in Table 2.

2.2 Mass loss

The corrosion products were chemically removed by placing the samples in a solution of

Table 2 Main environmental parameters of exposure site

Average annual temperature/°C	Average relative humidity/%	Average annual rainfall/mm	Rain days per year	Average total solar radiation/(W·m^{-2})	Deposition rate of Cl^-/(mg·m^{-2}·d^{-1})
28.1	81.6	2000	210	10	1154.25

50 mL H_3PO_4 + 20 g CrO_3 + 1 L H_2O for 5−10 min at 80 °C. The samples were then carefully washed with deionized water, dehydrated with alcohol, and dried in a cold air flow. Finally, the samples were weighed to obtain their final mass using an analytical balance.

2.3 Morphology observation

The surface and cross-section morphologies of the pure aluminum after 5, 13, 21 and 34 months of exposure were observed by SEM (QYANTA 450, FEI). The sample used for the cross-section observation was mounted with epoxy resin, ground down to 2000 girt SiC paper and lightly polished with a 1.0 μm diamond paste. Before observation, a layer of carbon was deposited onto the surface of the sample to enhance the conductivity of the oxide scale. In addition, the pit sizes were measured by white-light interferometer (MicroXAM) after removal of the corrosion products.

2.4 Composition analysis

After retrieving the samples, the compositions of the corrosion products were analyzed by XPS (ESCALAB250). All XPS peaks were calibrated using standard carbon contamination (284.6 eV). The data analysis was performed by the XPS PEAK 4.1 software.

2.5 Electrochemical measurements

Samples, with the dimensions of 10 mm × 10 mm, were used for electrochemical measurements. All electrochemical measurements were conducted with a PARSTAT 2273 electrochemical workstation in a conventional three-electrode cell, with a platinum sheet as the counter electrode and a saturated calomel electrode (saturated with KCl) as the reference electrode. To minimize the impact on the surface state of the samples, the electrolyte was 0.1 mol/L Na_2SO_4 (pH=5). The EIS measurements were performed over a frequency range of 100 kHz to 10 mHz using a signal amplitude perturbation of 10 mV. The EIS data were then fitted by the ZSimpWin software.

3 Results and discussion

3.1 Corrosion rate

Mass loss measurement is one of the most direct methods for evaluating the corrosion rate of material. Figure 1 shows the mass loss and corrosion rate of pure aluminum 1060 as a function of exposure time. From Fig. 1(a), it is obvious that the mass loss of the samples increases with time. In addition, the corrosion rate of the samples for different exposure periods can be calculated using the following relationship [11]:

$$V_n=\frac{12(w_n-w_{n-1})}{t_n-t_{n-1}} \tag{1}$$

where V is the corrosion rate (g·m^{-2}·a^{-1}), w is the mass loss (g·m^{-2}), t is the exposure time (month), and n is the period of sampling (n=1, 2, 3, and 4 refer to 5, 13, 21, and 34 months of exposure, respectively). As shown in Fig. 1(b), the corrosion rate decreases with an increase in the exposure time for the first 21 months, and then increases as the exposure time increases. After 13 months of corrosion, the corrosion rate is 1.28 g/(m^2·a^1). In addition, the corrosion rate of pure aluminum during one year of exposure in Qingdao (northern latitude 36°06′, eastern longitude 120°25′) is 0.54 g/(m^2·a^1) [18]. Compared with that in Qingdao, the corrosion attack of pure aluminum in Nansha Islands is much severer, indicating that the atmospheric environment is relatively harsh.

3.2 Analysis of corrosion products

To determine the composition of the corrosion products, surface analysis has been carried out by XPS. In particular, the sample surfaces were sputtered for 60 s before the test, to remove the contaminant layer on the surfaces during the field exposure tests. All results are obtained after sputtering for 60 s.

Figure 2 exhibits the XPS analysis of Al 2p on the surfaces of samples as a function of exposure time. The XPS spectra of Al 2p have a peak at

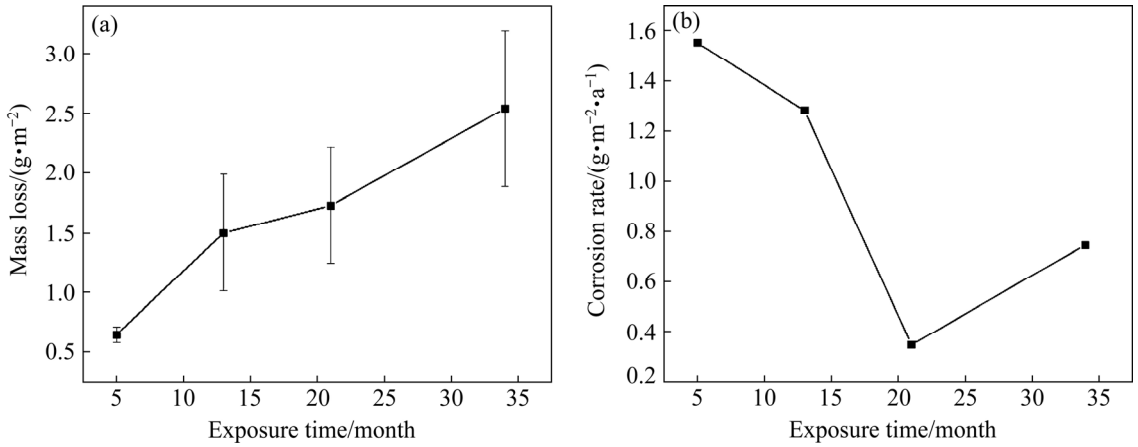

Fig. 1 Mass loss of pure aluminum 1060 exposed to Nansha Islands marine atmosphere at different time (a) and instantaneous corrosion rate as function of exposure time (b)

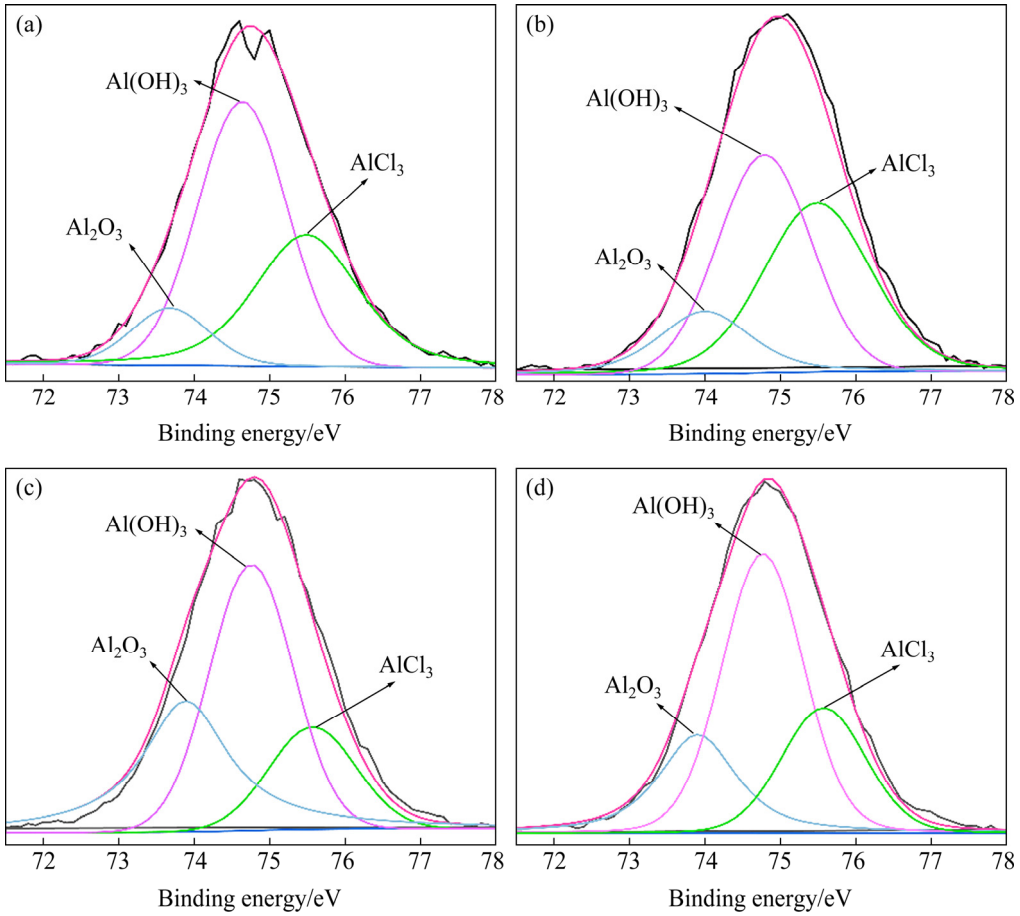

Fig. 2 XPS spectra of Al 2p for corrosion products formed on pure aluminum after different exposure time: (a) 5 months; (b) 13 months; (c) 21 months; (d) 34 months

about 75 eV (relative to C 1s = 284.6 eV), which corresponds to oxidized Al (Al^{3+}) [19]. After deconvolution of the core-level Al 2p spectra, three peaks are obtained, as shown in Fig. 2. The peaks at the binding energies of 73.8, 74.7 and 75.5 eV correspond to Al_2O_3, $Al(OH)_3$ and $AlCl_3$ [20,21], respectively.

Figure 3(a) shows the XPS spectra of Cl 2p on the surfaces of pure aluminum as a function of exposure time. The spectra show that there is a small amount of Cl^- in the corrosion products, as detected by XPS. Figure 3(b) shows the O 1s

spectra which are insensitive to exposure time, indicating that the corrosion products of oxygen do not significantly change with the time. Figure 4 shows the deconvolution of the core-level O 1s spectra. The O 1s spectra can be assigned to 530.3, 531.7 and 533.0 eV, which are attributed to O^{2-}, OH^- and H_2O, respectively [22]. Combined with the Al 2p spectra, it is evident that the corrosion product layer consists mainly of $Al(OH)_3$, which is similar to the generally accepted corrosion products of aluminum [23].

3.3 Morphology of corrosion products

The surface morphologies of the corrosion products change gradually with an increase in exposure time. It can be seen with the naked eye

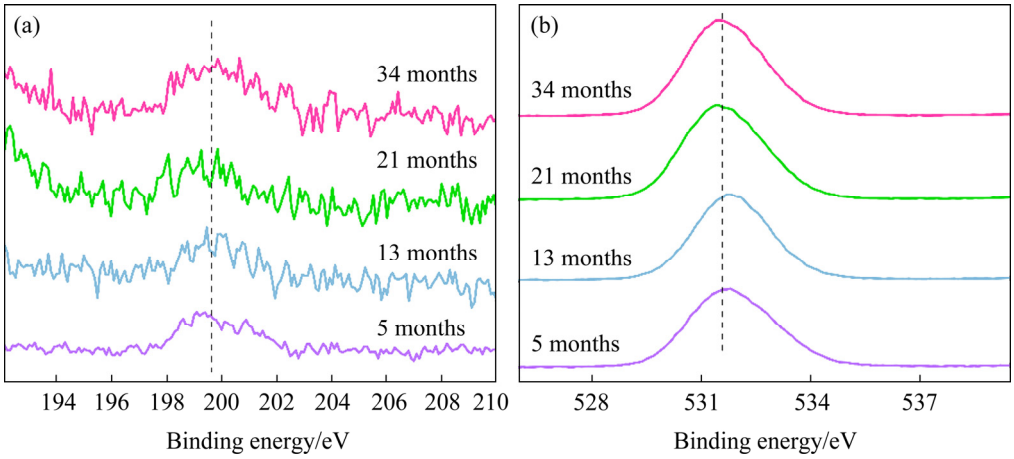

Fig. 3 XPS spectra of Cl 2p (a) and O 1s (b) for corrosion products formed on pure aluminum after different exposure time

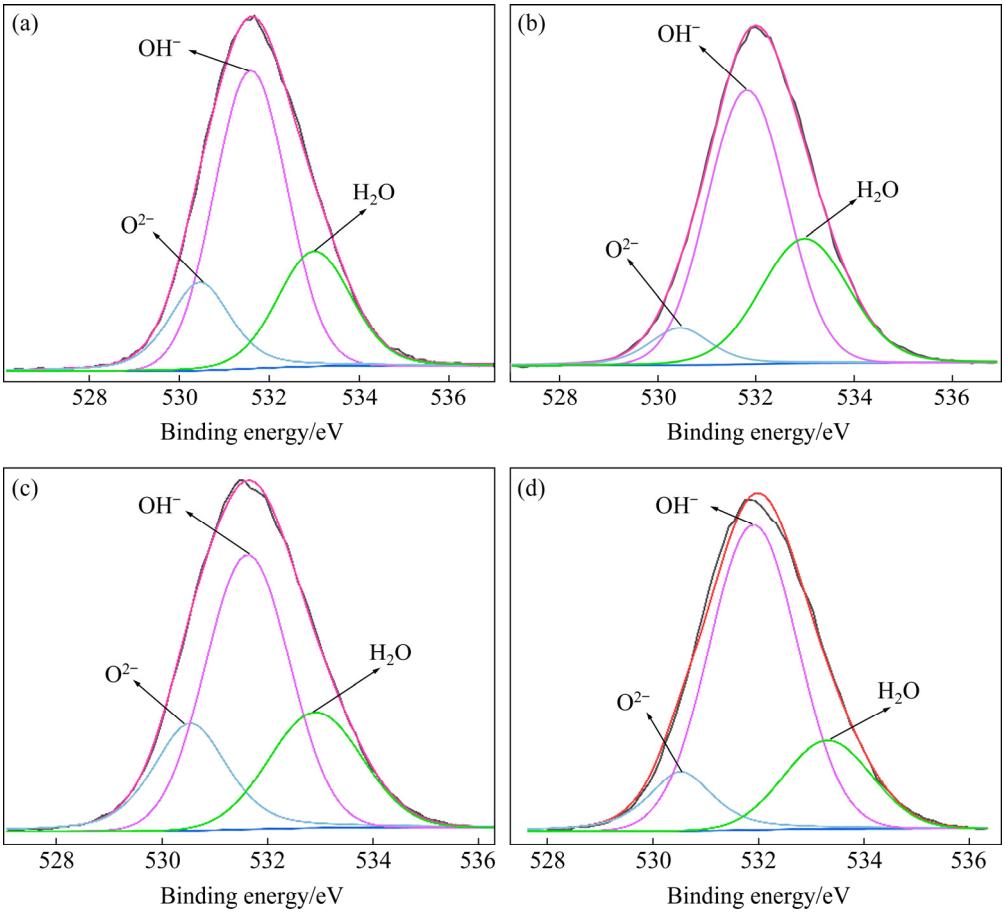

Fig. 4 Deconvolution of core-level O 1s XPS spectra for corrosion products formed on pure aluminum after different exposure time: (a) 5 months; (b) 13 months; (c) 21 months; (d) 34 months

that the samples have lost their original bright metallic color and developed some spots which are visually identified as corrosion products after exposure. Figure 5 shows the evolution of the microscopic morphologies of pure aluminum for different exposure periods in Nansha Islands. In Fig. 5(a), after 5 months of exposure, the corrosion products are independent and discrete, and the substrate is clearly visible. From a close look, it can be observed that cracks appear below the corrosion products, as indicated by red arrows. After 13 months of exposure, many crack-like corrosion products have appeared. So many corrosion products piled on the surfaces of the samples that the substrate can hardly be seen. It is also noteworthy that there are some pores caused by pitting corrosion (marked with red arrows) on the surfaces after exposure for 13, 21 and 34 months, and around them, a large amount of corrosion products are found. According to the EDS results in Table 4, the elemental compositions of the corrosion products typically include Al and O. In addition, certain amounts of Mg and S are also detected, which are caused by salt sprays [10]. The presence of salt sprays causes the air to contain a large amount of salts (including NaCl, Na_2SO_4, and $MgCl_2$). These salts are deliquescent and absorb moisture, and can easily form a thin electrolyte film, which accelerates the corrosion of aluminum [24−27].

The cross-sectional morphology of the pure aluminum exposed for 34 months is presented in Fig. 6. It shows that pitting corrosion occurs at a depth of approximately 38.8 μm. According to the cross-section morphology, it is determined to be a subcutaneous pit, and corrosion products are trapped inside the cavity. The EDS results show that it mainly contains Al and O. Typically, there are many tiny cracks in the corrosion products, and these cracks have extended to the matrix. This indicates that further corrosion of the substrate may occur.

3.4 Pitting corrosion

The surface morphologies of the samples exposed to Nansha Islands for different periods after the removal of the corrosion products are shown in Fig. 7. Corrosion is, mainly pitting corrosion, including deep and shallow pits. The discrete and shallow pits observed in Fig. 7(a) after 5 months of exposure may be due to active dissolution of the substrate. According to the passivation and repassivation theory, pitting corrosion is a dynamic competitive process between the dissolution of the substrate and the formation of protective oxide film (repassivation). Oxygen is

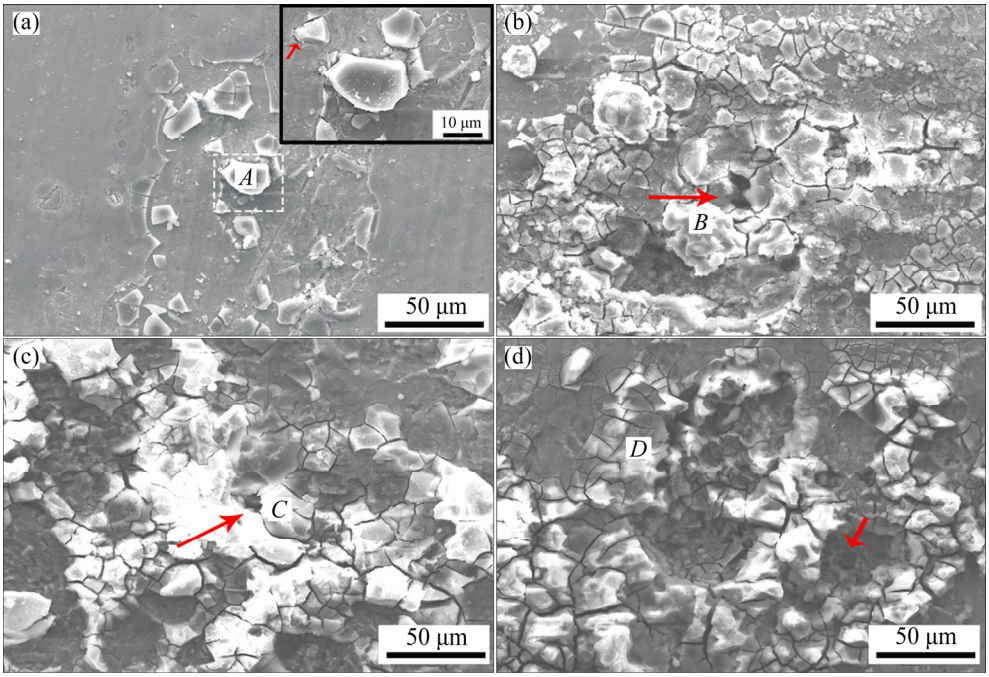

Fig. 5 Surface morphologies of corrosion products formed on pure aluminum after different exposure time: (a) 5 months; (b) 13 months; (c) 21 months; (d) 34 months

Table 4 EDS results of Regions *A*, *B*, *C* and *D* on aluminum surfaces after different exposure time (wt.%)

Region	O	Al	Mg	S
A	28.45	63.15	2.52	5.89
B	38.30	48.12	0.94	12.64
C	35.66	49.72	2.41	12.21
D	43.47	43.56	1.62	11.35

necessary to repair the oxide film and facilitate repassivation [28]. After 5 months of exposure, the damaged oxide film can be repaired in time. Therefore, shallow and isolated pits are formed. In addition, fresh pits can initiate at the edge of repassivated pits [29,30], allowing the pits to coalesce into larger or wider pits. This is confirmed in Fig. 7(b). The corrosion products continue to accumulate over time. It is easy to attain anoxic conditions beneath pits. Pitting corrosion is considered to be controlled by an autocatalytic process under the anoxic conditions [31], in which aluminum oxidation is the anode reaction and the formation of hydrogen is the cathode reaction. According to the acidification mechanism proposed by GALVELE [32], when *xi* (*x* represents the pit depth and *i* is the current density at the pit bottom) exceeds a critical value, the pit propagates. In addition, the greater the value of *xi*, the more difficult to repassivate. From Evans diagram, it can be inferred that the corrosion current density during the hydrogen evolution reaction is higher than that during oxygen reduction. As a result, the pits become wider and larger with time, as confirmed by Figs. 7(c) and (d). In particular, at a higher magnification (Fig. 7(e)), geometric facets are observed in pits with irregular shapes (marked with red arrows), and the side of the facets are estimated to be approximately 1 μm.

In order to further observe the evolution of the pits with different exposure periods, the statistical

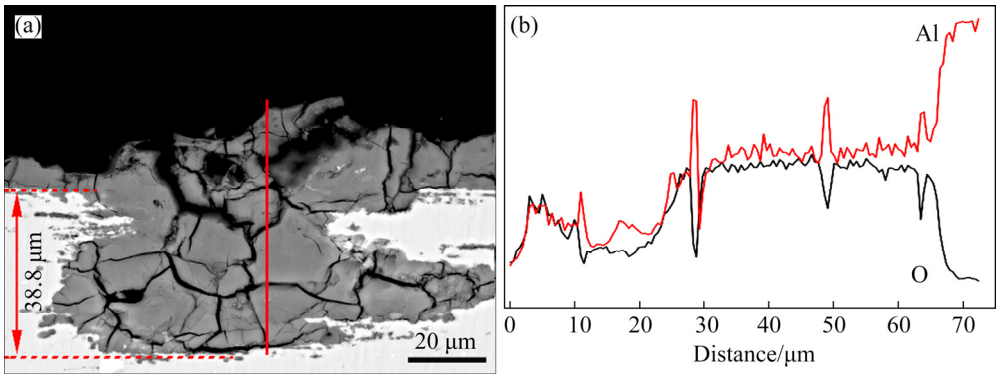

Fig. 6 Cross-sectional morphology (a) and EDS results (b) of corrosion products after 34 months of exposure

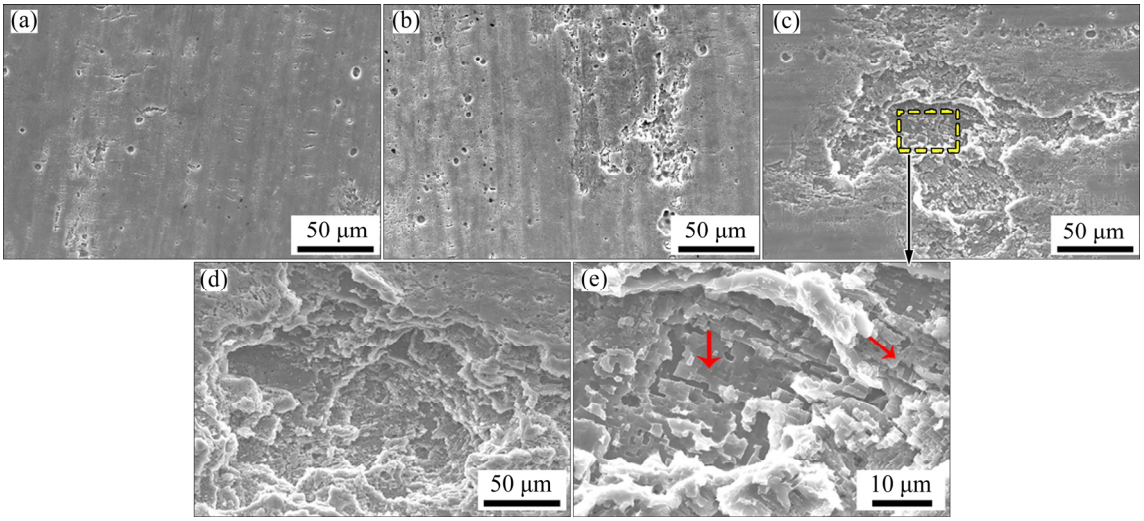

Fig. 7 Surface morphologies of pure aluminum 1060 exposed for different time after removing corrosion products: (a) 5 months; (b) 13 months; (c) 21 months; (d) 34 months; (e) Magnified view of pit in (c)

distributions of the 2D sizes of the pits are shown in Fig. 8. The mean rank method is used to calculate the cumulative probability of the geometry parameters (diameter and depth) of the pits [33,34], that is $P=n/(N+1)$, where N is the total number of the pits, and n is the order of the total number. The median of the distribution (diameter and depth) of the pits for different exposure time is simply determined at P=50%, and the statistical results are shown in Fig. 8. With an increase in exposure time, the mean width and depth of the pits increase continuously, and the final width and depth of the pits reach 5.441 and 6.286 μm, respectively, indicating that the pits expand in both the parallel and vertical directions. The following equations can be used to describe the geometry of a pit [35]: $D/(2h)>1$, the pit is wide-shallow in shape; $D/(2h)=1$, the pit is semi-spherical in shape; $D/(2h)<1$, the pit exhibits a narrow-shallow shape, where D and h represent the width and depth of the pit, respectively. For samples exposed to Nansha Islands for 5, 13, 21 and 34 months, the $D/2h$ values are 0.336, 0.377, 0.414, and 0.433 in turn, indicating that the pits are narrow-shallow in shape, and tend to expand with an increase in corrosion time.

3.5 Electrochemical results

EIS is recorded at the stable open circuit potential to investigate the protection of the corrosion products after different exposure time. The results are presented in terms of both the Nyquist and Bode diagrams in Fig. 9. The Nyquist diagram of the uncorroded sample shows a single capacitive arc, and the semicircle is much smaller. For the corroded samples, a second capacitive loop is observed. Significantly, the semicircles increase during the first 13 months of exposure and then decrease with an increase in exposure time. From the Bode plots, the maximum peak angles appearing at high frequency are related to the corrosion product film, and the peak angles in the low frequency may be ascribed to the electric double layer. It is clear that the samples exposed for 13 months or longer show distinct peaks in the high frequency region, indicating the formation of

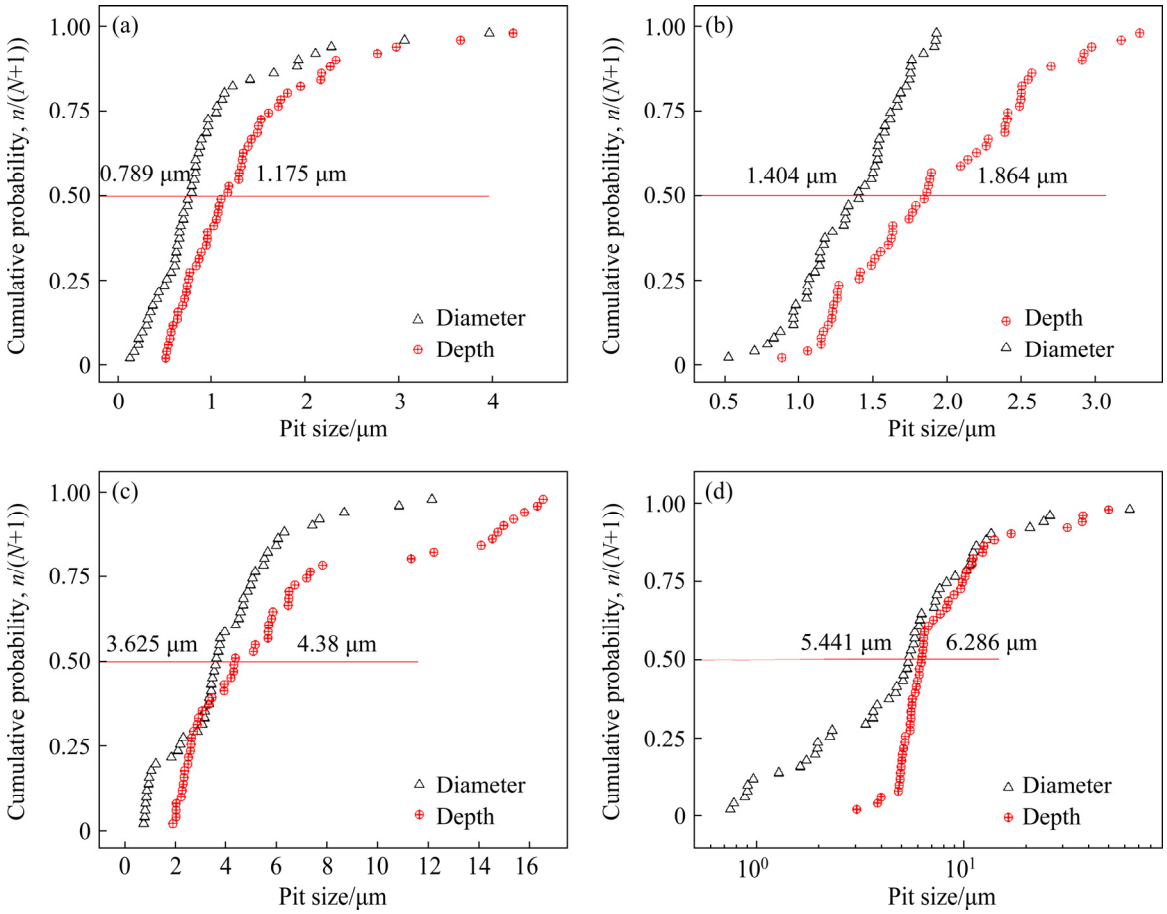

Fig. 8 Statistical distributions of 2D sizes of pits after different exposure time: (a) 5 months; (b) 13 months; (c) 21 months; (d) 34 months

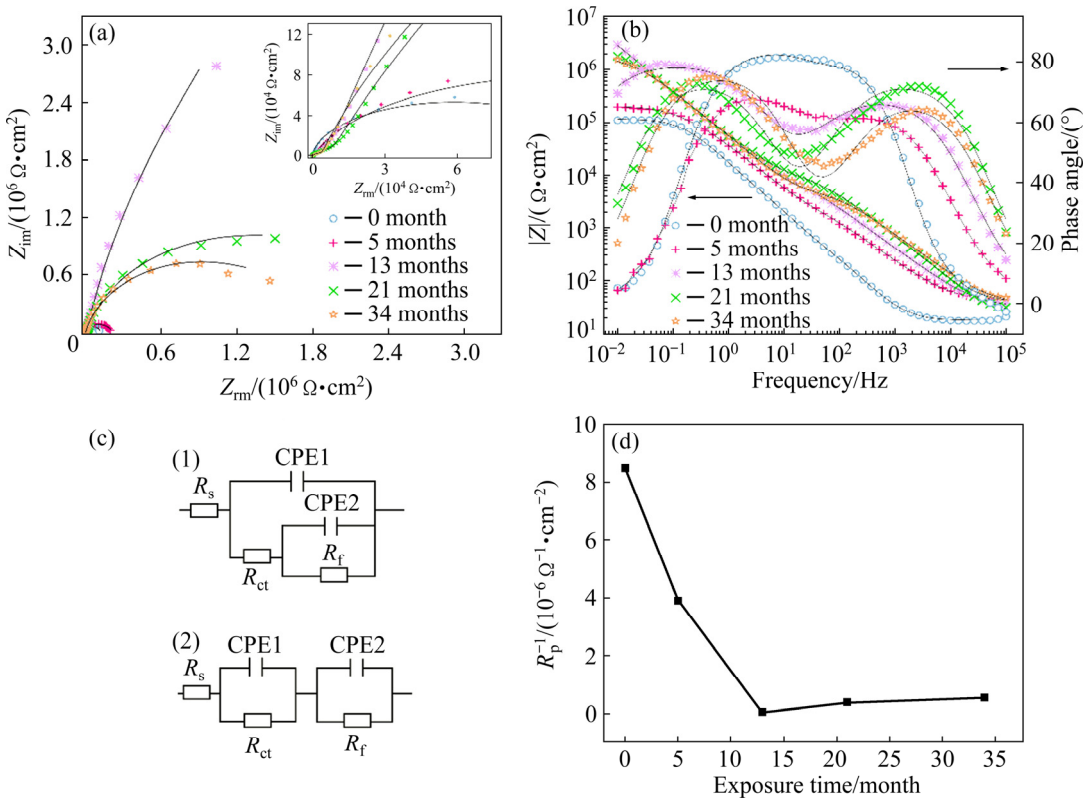

Fig. 9 Nyquist plots (a) and Bode plots (b) after different exposure time, equivalent circuits used for fitting EIS data (c), and variation of $1/R_p$ after different exposure time (d)

corrosion product layer. Equally, there are noticeable peaks in the low frequency region, indicating that the charge transfer process is inhibited.

To describe the sub-electrochemical interface process in detail, reasonable fitting models are proposed, as shown in Fig. 9(c). The equivalent circuit assumes that the corrosion product layer does not completely cover the surface of the substrate and cannot be considered as a uniform layer, but rather as a defect layer [35]. Therefore, a constant phase element (CPE) is used to replace the ideal capacitance element due to the heterogeneity of the electrode surfaces. Once exposed to air, a layer of oxide film forms rapidly on the surface of aluminum. Thus, it can be assumed that there is an initial oxide film on the surfaces of the unexposed samples. After 5 months of exposure, the oxide film is destroyed locally and the corrosion products are randomly distributed on the surfaces. With an increase in exposure time, a compact corrosion product layer is formed. In particular, after 21 and 34 months of exposure, the corrosion products continue to peel, and the corrosion product layer is no longer dense. In equivalent circuit (1), the oxide film or corrosion product layer is speculated to have a porous structure [36]. In contrast, the corrosion product layer has a compact structure in the equivalent circuit (2). Therefore, equivalent circuit (1) is suitable for samples after 0, 5, 21 and 34 months of exposure, and equivalent circuit (2) is suitable for samples after 13 months of exposure. The fitted parameters are presented in Table 5.

In the equivalent circuit (1), a pair of elements in parallel, namely CPE1 (the double electric layer) and R_{ct} (charge transfer resistance), represent the dielectric properties of the electric double layer at the interface between the corrosion product layer and the solution. Another pair of CPE2 (film capacitance) and R_f (film resistance) describe the charge transfer process through the corrosion product layer. The equivalent circuit (2) also models two time constants, including an electric double layer (CPE1 and R_{ct}) and a compact and protective corrosion product layer (CPE2 and R_f). Notably, the chi-square value (χ^2) is very small, indicating that the fitted data are relatively accurate. In this study, the reciprocal of the polarization resistance $1/R_p$ is

used as a parameter for characterizing the corrosion rate of pure aluminum [37,38], as shown in Fig. 9(d). It can be seen that the value of $1/R_p$ decreases during the first 13 months of exposure and then remains at a small value, indicating that the corrosion products layer is protective. In other words, a further increase in the corrosion time after 13 months of exposure results in a lower corrosion rate. This result is consistent with the measured corrosion rate.

3.6 Formation of corrosion products on pure aluminum 1060

When exposed to air, aluminum forms a layer of oxide film with a thickness of few nanometers. For the most natural solutions, the oxide film has a positive surface charge, and is prone to adsorb Cl^- due to the coulombic interactions [12]. This process is illustrated in Fig. 10(a). Using autoradiography, BERZINS et al [39] found that the adsorption of Cl^- is highly localized and corresponds to the location of the pits. Once Cl^- is adsorbed onto the surface, it has ample opportunity to react with the oxide film. There is a growing body of evidence that Cl^- penetrates oxide film, and several possible mechanisms have been proposed [12]: (1) Cl^- penetrates the oxide film through oxygen vacancies; (2) Cl^- penetrates the oxide film through water channels; (3) localized dissolution or thinning of the oxide film occurs. On the one hand, alumina

Table 5 EIS fitted parameters of un-corroded and corroded samples after different exposure time

Exposure time/ month	R_s/ ($\Omega\cdot$ cm^2)	Q_{dl}/ ($\Omega^{-1}\cdot$cm$^{-2}\cdot$S^{-n})	n_{dl}	R_{ct}/ ($\Omega\cdot$cm^2)	Q_f/ ($\Omega^{-1}\cdot$cm$^{-2}\cdot$S^{-n})	n_f	R_f/ ($\Omega\cdot$cm^2)	$\Sigma\chi^2$/ 10^{-3}
0	17.74	8.465	0.949	3.46×10^3	1.394	0.943	1.14×10^5	1.883
5	41.68	4.238	0.793	5.09×10^3	1.588	0.908	2.05×10^5	1.675
13	31.84	4.150	0.761	5.69×10^3	3.919	0.888	2.03×10^7	0.989
21	23.10	0.911	0.841	1.25×10^4	2.810	0.855	2.58×10^6	4.107
34	34.97	0.012	0.799	6.11×10^3	2.502	0.900	1.84×10^6	4.492

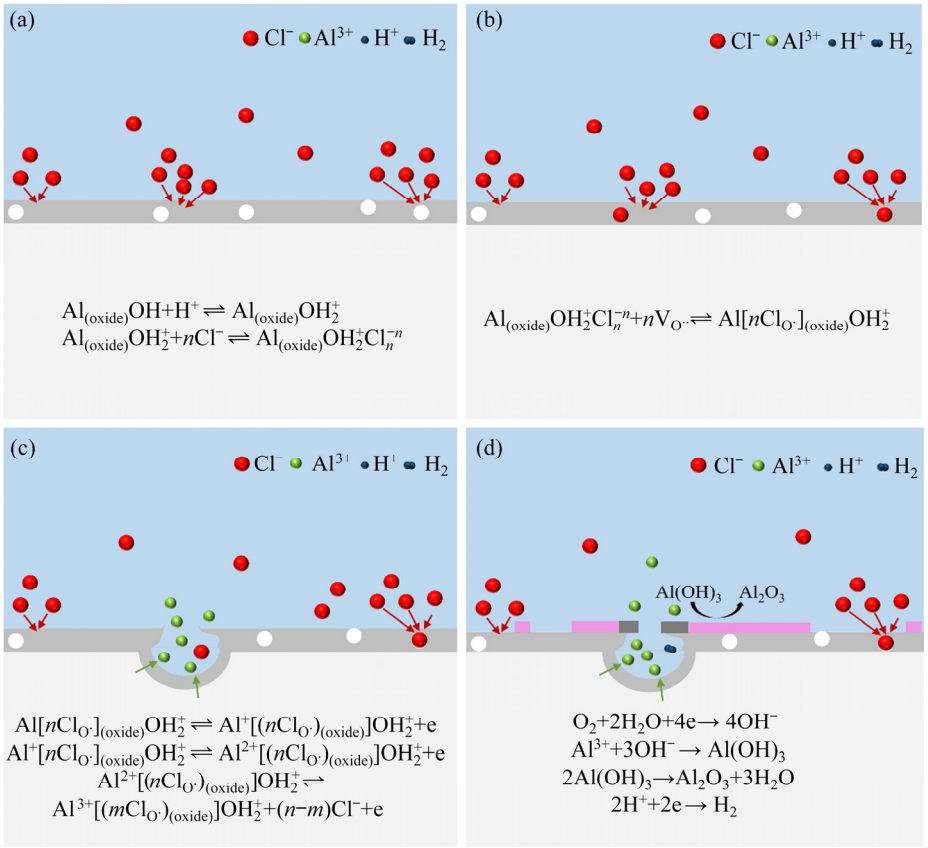

Fig. 10 Schematic of pitting corrosion mechanism of pure aluminum 1060 exposed to Nansha Islands marine atmosphere environment

behaves as an *n*-type semiconductor [40,41], and the donors are mainly oxygen vacancies; on the other hand, the radius of Cl^- is only slightly larger than that of O^{2-} [12] (1.81 vs. 1.40 Å, respectively). Therefore, it is reasonable to assume that Cl^- penetrates the oxide film through oxygen vacancies and leads to corrosion. This process is described in Figs. 10 (b) and (c).

In atmospheric corrosion, oxygen can easily approach the metal surface. Therefore, the main cathodic reaction at the cathode site is the oxygen reduction reaction:

$$O_2+2H_2O+4e\rightarrow 4OH^- \quad (2)$$

As the local pH increases as a result of the cathodic oxygen reduction reaction, the following reaction occurs:

$$Al^{3+}+3OH^-\rightarrow Al(OH)_3 \quad (3)$$

$Al(OH)_3$ further transforms into Al_2O_3 via the following reaction:

$$2Al(OH)_3\rightarrow Al_2O_3+3H_2O \quad (4)$$

This process is described in Fig. 10(d). Therefore, the main corrosion products are Al_2O_3 and $Al(OH)_3$.

Similarly, chlorides also exist in the corrosion product layer and Cl^- participates in the reaction. This process can be described in the following sequence of reactions [42]:

$$Al(OH)_3+Cl^-\rightarrow Al(OH)_2Cl+OH^- \quad (5)$$

$$Al(OH)_2Cl+Cl^-\rightarrow Al(OH)Cl_2+OH^- \quad (6)$$

$$Al(OH)Cl_2+Cl^-\rightarrow AlCl_3+OH^- \quad (7)$$

The Cl^- replaces the OH^- in the $Al(OH)_3$ to form $AlCl_3$ constantly by competitive adsorption. Cl^- is mainly present in the form of $AlCl_3$ in the corrosion products. As shown in our XPS results in Fig. 2, there is always a small amount of $AlCl_3$ present in the corrosion products after exposure. In this case, the corrosion products are composed of Al_2O_3, $Al(OH)_3$ and $AlCl_3$.

4 Conclusions

(1) Nansha Islands is a harsh marine atmospheric environment. The average corrosion rate of pure aluminum exposed for 13 months is approximately 1.28 g/(m^2·a).

(2) Pitting corrosion is the main corrosion form for pure aluminum and is initiated with some metastable pits, which then gradually develops into stable pits in Nansha Islands marine atmospheric environment.

(3) The pits are narrow and shallow in shape, and tend to expand with an increase in corrosion time. In addition, the mean width and depth of the pits increase continuously, and the final width and depth reach 5.441 and 6.286 μm, respectively.

(4) The corrosion products formed on the surface of pure aluminum are more protective than the native oxide film, and the protectiveness first increases and then decreases with the continuation of corrosion process.

Acknowledgments

This work was supported by the National Natural Science Foundation of China (No. 51671197), and Special Project of Chinese Academy of Sciences (No. XDA130040502).

References

[1] LIU Y W, ZHAO H T, WANG Z Y, WEI Y H, PAN C, LV C X. Corrosion behavior of low-carbon steel and weathering steel in a coastal zone of the Spratly islands: A tropical marine atmosphere [J]. International Journal of Electrochemical Science, 2020, 15(7): 6464−6477.

[2] LU X, LIU Y W, ZHAO H T, PAN C, WANG Z Y. Corrosion behavior of copper in extremely harsh marine atmosphere in Nansha Islands, China [J]. Transactions of Nonferrous Metals Society of China, 2021, 31(3): 703−714.

[3] NATESAN M, VENKATACHARI G, PALANISWAMY N. Kinetics of atmospheric corrosion of mild steel, zinc, galvanized iron and aluminium at 10 exposure stations in India [J]. Corrosion Science, 2006, 48(11): 3584−3608.

[4] LIU Y J, WANG Z Y, KE W. Study on influence of native oxide and corrosion products on atmospheric corrosion of pure Al [J]. Corrosion Science, 2014, 80: 169−176.

[5] MENDOZA A R, CORVO F. Outdoor and indoor atmospheric corrosion of non-ferrous metals [J]. Corrosion Science, 2000, 42(7): 1123−1147.

[6] LU X, LIU Y W, ZHAO H T, WANG Z Y. Corrosion behavior of brass H62 in harsh marine atmosphere in Nansha Islands, China [J]. Journal of Materials Engineering and Performance, 2020, 29(12): 8156−8164.

[7] NATISHAN P M, O'GRADY W E. Chloride ion interactions with oxide-covered aluminum leading to pitting corrosion: A review [J]. Journal of the Electrochemical Society, 2014, 161(9): C421−C432.

[8] LIANG M X, MELCHERS R, CHAVES I. Corrosion and pitting of 6060 series aluminium after 2 years exposure in seawater splash, tidal and immersion zones [J]. Corrosion Science, 2018, 140: 286−296.

[9] LU X, LIU Y W, LIU M R, WANG Z Y. Corrosion behavior of copper T2 and brass H62 in simulated Nansha marine

atmosphere [J]. Journal of Materials Science & Technology, 2019, 35(9): 1831−1839.

[10] ZHOU S G, YAN Q Q, TANG C T, MAO F X, PU J B, MACDONALD D D. Effect of the chloride on passivity breakdown of Al−Zn−Mg alloy [J]. Corrosion Science, 2020, 163: 108254.

[11] CUI Z Y, LI X G, XIAO K, DONG C F, LIU Z Y, ZHANG D W. Atmospheric corrosion behaviour of pure Al 1060 in tropical marine environment [J]. Corrosion Engineering Science and Technology, 2015, 50(6): 438−448.

[12] MCCAFFERTY E. Sequence of steps in the pitting of aluminum by chloride ions [J]. Corrosion Science, 2003, 45(7): 1421−1438.

[13] WANG B B, WANG Z Y, HAN W, KE W. Atmospheric corrosion of aluminium alloy 2024-T3 exposed to salt lake environment in Western China [J]. Corrosion Science, 2012, 59: 63−70.

[14] CAO M, LIU L, FAN L, YU Z F, LI Y, OGUZIE E E, WANG F H. Influence of temperature on corrosion behavior of 2A02 Al alloy in marine atmospheric environments [J]. Materials, 2018, 11(2): 235.

[15] RODRÍGUEZ J J S, HERNÁNDEZ F J S, GONZÁLEZ J E G. The effect of environmental and meteorological variables on atmospheric corrosion of carbon steel, copper, zinc and aluminium in a limited geographic zone with different types of environment [J]. Corrosion Science, 2003, 45(4): 799−815.

[16] CAO M, LIU L, YU Z F, FAN L, LI Y, WANG F H. Electrochemical corrosion behavior of 2A02 Al alloy under an accelerated simulation marine atmospheric environment [J]. Journal of Materials Science & Technology, 2019, 35(4): 651−659.

[17] LIU Y, MENG G Z, CHENG Y F. Electronic structure and pitting behavior of 3003 aluminum alloy passivated under various conditions [J]. Electrochimica Acta, 2009, 54(17): 4155−4163.

[18] ZHENG Qi-fei, SUN Shuang-qing, WEN Jun-guo. Analysis of atmospheric corrosion of aluminum and aluminum alloys and its influencing factors in China [J]. Corrosion & Protection, 2009, 30(6): 359−363. (in Chinese)

[19] BOCKRIS J O, KANG Y K. The protectivity of aluminum and its alloys with transition metals [J]. Journal of Solid State Electrochemistry, 1997, 1(1): 17−35.

[20] WANG B, ZHANG L W, SU Y, MOU X L, XIAO Y, LIU J. Investigation on the corrosion behavior of aluminum alloys 3A21 and 7A09 in chloride aqueous solution [J]. Materials & Design, 2013, 50: 15−21.

[21] BUCKO M, BASTOS A C, YASAKAU K A, FERREIRA M G S, BAJAT J B. Corrosion behavior of AA2024-T6 and AA6065-T6 alloys in reline [J]. Electrochimica Acta, 2020, 357: 136861.

[22] YANG Y, ZENG H T, XIN S S, HOU X L, LI M C. Electrochemical corrosion behavior of 2205 duplex stainless steel in hot concentrated seawater under vacuum conditions [J]. Corrosion Science, 2020, 165: 108383.

[23] ZHANG S, ZHANG T, HE Y T, LIU D X, WANG J P, DU X, MA B L. Long-term atmospheric corrosion of aluminum alloy 2024-T4 in coastal environment: Surface and sectional corrosion behavior [J]. Journal of Alloys and Compounds, 2019, 789: 460−471.

[24] MORCILLO M, CHICO B, ALCÁNTARA J, DÍAZ I, SIMANCAS J, de LA FUENTE D. Atmospheric corrosion of mild steel in chloride-rich environments: Questions to be answered [J]. Materials and Corrosion-Werkstoffe Und Korrosion, 2015, 66(9): 882−892.

[25] AHMAD Z, ALLAM I M, ABDUL ALEEM B J. Effect of environmental factors on the atmospheric corrosion of mild steel in aggressive sea coastal environment [J]. Anti-corrosion Methods and Materials, 2000, 47(4): 215−226.

[26] MA Y T, LI Y, WANG F H. Corrosion of low carbon steel in atmospheric environments of different chloride content [J]. Corrosion Science, 2009, 51(5): 997−1006.

[27] PROSEK T, THIERRY D, TAXÉN C, MAIXNER J. Effect of cations on corrosion of zinc and carbon steel covered with chloride deposits under atmospheric conditions [J]. Corrosion Science, 2007, 49(6): 2676−2693.

[28] de LA FUENTE D, OTERO-HUERTA E, MORCILLO M. Studies of long-term weathering of aluminium in the atmosphere [J]. Corrosion Science, 2007, 49(7): 3134−3148.

[29] SOLTIS J. Passivity breakdown, pit initiation and propagation of pits in metallic materials — Review [J]. Corrosion Science, 2015, 90: 5−22.

[30] MELCHERS R E. Bi-modal trend in the long-term corrosion of aluminium alloys [J]. Corrosion Science, 2014, 82: 239−247.

[31] FRANKEL G S. Pitting corrosion of metals—A review of the critical factors [J]. Journal of the Electrochemical Society, 1998, 145(6): 2186−2198.

[32] GALVELE J. Transport processes in passivity breakdown. II. Full hydrolysis of the metal ions [J]. Corrosion Science, 1981, 21(8): 551−579.

[33] SHIBATA T, ZHU Y C. The effect of film formation temperature on the stochastic-processes of pit generation on anodized titanium [J]. Corrosion Science, 1994, 36(10): 1735−1749.

[34] SHIBATA T, AMEER M A M. Stochastic-processes of pit generation on zirconium with an anodic oxide film [J]. Corrosion Science, 1992, 33(10): 1633−1643.

[35] HU S B, LIU R, LIU L, CUI Y, OGUZIE E E, WANG F H. Effect of hydrostatic pressure on the galvanic corrosion of 90/10 Cu−Ni alloy coupled to Ti6Al4V alloy [J]. Corrosion Science, 2020, 163: 108242.

[36] CUI Z Y, WANG L W, NI H T, HAO W K, MAN C, CHEN S S, WANG X, LIU Z Y, LI X G. Influence of temperature on the electrochemical and passivation behavior of 2507 super duplex stainless steel in simulated desulfurized flue gas condensates [J]. Corrosion Science, 2017, 118: 31−48.

[37] CHUNG K W, KIM K B. A study of the effect of concentration build-up of electrolyte on the atmospheric corrosion of carbon steel during drying [J]. Corrosion Science, 2000, 42(3): 517−531.

[38] YIN Q, WANG Z Y, PAN C. Initial corrosion behavior of pure zinc in simulated tropical marine atmosphere [J]. Transactions of Nonferrous Metals Society of China, 2018, 28(12): 2582−2591.

[39] BERZINS A, EVANS J V, LOWSON R T. Aluminium corrosion studies. II. Corrosion rates in water [J]. Australian

Journal of Chemistry, 1977, 30(4): 721−731.
[40] MARTIN F J, CHEEK G T, O'GRADY W E, NATISHAN P M. Impedance studies of the passive film on aluminium [J]. Corrosion Science, 2005, 47(12): 3187−3201.
[41] PECH-CANUL M A, PECH-CANUL M I, BARTOLO-PÉREZ P, ECHEVERRÍA M. The role of silicon alloying addition on the pitting corrosion resistance of an Al−12wt.%Si alloy [J]. Electrochimica Acta, 2014, 140: 258−265.
[42] NGUYEN T H, FOLEY R T. The chemical nature of aluminum corrosion: III. The dissolution mechanism of aluminum oxide and aluminum powder in various electrolytes [J]. Journal of the Electrochemical Society, 1980, 127(12): 2563−2566.

纯铝 1060 在中国南沙群岛严酷海洋大气中的腐蚀以及点蚀行为

彭 灿[1,2]，刘雨薇[2,3]，郭明晓[1,2]，顾天真[1,2]，汪 川[2,3]，王振尧[2,3]，孙 成[2,3]

1. 中国科学技术大学 材料科学与工程学院，沈阳 110016；
2. 中国科学院 金属研究所，沈阳 110016；
3. 辽宁沈阳土壤大气环境材料腐蚀国家野外科学观测研究站，沈阳 110016

摘 要：通过质量损失测量、扫描电子显微术、能谱分析、X 射线光电子能谱和电化学阻抗谱等技术研究纯铝 1060 在南沙群岛海洋大气环境中暴露 34 个月后的腐蚀行为以及点蚀行为。结果表明，在纯铝表面发生严重的点蚀，并且暴露 13 个月后的平均腐蚀速率达到 1.28 g/(m^2·a)。X 射线光电子能谱的测试结果表明主要的腐蚀产物为 Al_2O_3、$Al(OH)_3$ 和 $AlCl_3$。此外，形成的腐蚀产物层相比于自然形成的氧化膜更具有保护作用，并且保护作用先增加然后降低。最后，蚀坑的形状通过统计分析的方法进行估计。

关键词：铝；大气腐蚀；南沙群岛；点蚀；户外暴露

(Edited by Xiang-qun LI)